We would like to thank the reviewer for your valuable comments that could further improve the quality of the paper. Please find below each reviewer comment in black and our response in red.

The manuscript investigates the role played by various data derived surface forcings in a Particle Tracking Model (PTM). The results are potentially interesting, but the paper needs major revision before publication. The main issues are indicated below, followed by more specific points.

Main Issues

1. The paper deals with a specific PTM, aimed at reproducing particles moving at the ocean surface and at 2 m depth. While this is a perfectly valid approach, I think the authors should clarify that this is not directly applicable to the transport of macro or micro plastic. Indeed, specific terms should be added to the PTM to simulate the behaviour of plastic debris, depending on their size and characteristics. Such processes include fragmentation, buoyancy changes due to colonization, aggregation and several others. The authors should explain this point up front in the Introduction and Conclusions, i.e. that they focus only on the fluid dynamical part of plastic transport, while for actual applications a number of other processes should included.

Thank you for this important comment. We agree that the scope of the PTM should be clearly distinguished from a complete macroplastic or microplastic fate model. In the revised manuscript, we have clarified this point in the Introduction, Methods, and Conclusions. Specifically, we now state in the Introduction that "floating debris transport" in this study refers to the fluid-dynamical transport component represented by passive particles moving near the ocean surface, rather than the complete fate of specific macroplastic or microplastic particles. We also explicitly state that particle-specific processes such as fragmentation, biofouling-induced buoyancy change, aggregation, settling, and resuspension were not included in the present framework (Lines 78-81, Lines 85-89, Lines 717-723).

2. I am worried about the drifters used in the experiment. No details on drifter testing is provided in Section 2.1, and it is well known that drifters with different properties can move very differently, especially in the very upper part of the ocean. In particular, windage and Stokes drift can be very sensitive to the surface expression. It is important that the authors provide information on the fluid dynamical properties of drifter motion, either using lab experiments or at least quantitatively comparing their motion with that of other drifters with tested properties (such as for instance CODE or CARTHE for the 2m case).

Thank you for this important comment. We agree that the fluid-dynamical properties of the drifters should be described more clearly, because near-surface drifter motion can be sensitive to drifter geometry, surface expression, windage, and Stokes drift. We have therefore revised Section 2.1 and the related Methods sections to provide a more quantitative description of the drifter geometry, effective sampling depth, and windage coefficients. We did not perform laboratory calibration experiments for these custom-made drifters, and we now state this limitation explicitly in the manuscript. Instead, we added a quantitative geometry-based comparison with tested near-surface drifter designs, including previous conventional design including CODE and CARTHE drifters.

DX drifter was 0.30 m high and 0.09 m in diameter, with 0.03–0.05 m protruding above the sea surface, and the DO drifter additionally included two 0.30 × 0.30 m perpendicular drogue plates positioned near 2 m depth. the effective sampling depth for the DO drifter was estimated from the area-weighted hydrodynamic centroid of the submerged cylindrical body and the drogue. The submerged cylindrical body has a projected area of approximately $0.09 \times 0.26 = 0.0234\ \mathrm{m}^2$, with its centroid near 0.13 m depth, whereas one effective 0.30 × 0.30 m drogue plate has a projected area of $0.09\ \mathrm{m}^2$, centered near 2 m depth. Therefore, $z_c = [(0.0234)(0.13) + (0.09)(2.0)]/(0.0234 + 0.09) \approx 1.6$ m. Thus, the adopted effective depth of $z = -1.5$ m for the DO Stokes drift and Ekman current provides a reasonable representation of the combined hydrodynamic response of the surface float and submerged drogue.

The CARTHE drifter follows currents in the upper 0.60 m of the water column, with a representative drogue depth of approximately 0.40 m and wind-induced slip less than 0.5% of the 10 m wind speed (Novelli et al., 2017; Poulain et al., 2022). The CARTHE drogue dimension of 0.38 × 0.38 m was taken from the drifter drag-area comparison reported by McCaffrey and Koeberle (2024). The CODE drifter is a standard upper-ocean surface drifter designed to measure currents in the upper meter of the water column using four drag-producing sails attached to a vertical body (Davis, 1985; Poulain et al., 2022). The effective depth of the CODE drifter was set to approximately 0.5 m, and its mean downwind slip has been reported to be about 0.1% of the wind speed (Poulain and Gerin, 2019). We have added this in Lines 104-113.

Table R1. Comparison of the custom DX/DO drifters with tested near-surface drifter designs.

Drifter type	Shape	Dimensions	Effective depth	Windage coefficient
DX, this study	Cylinder	0.30 m high; 0.09 m diameter	~0.135 m	0.015
DO, this study	Cylinder + drogue plate	DX body + two 0.30 × 0.30 m plates near 2 m depth	~1.6 m	0.005
CARTHE	Toroid + drogue plate	0.38 × 0.38 m drogue	~0.4 m	< 0.005
CODE	Sails	1 m-long tube; sail top ~0.30 m below surface	~0.5 m	~0.001

3. The explanation of the datasets and schemes used in the analysis (Section 2.2-2.3) is incomplete and not very clear.

Please explain further the characteristic of the SEALEVEL product, in particular from which satellite observations is obtained and what is the expected physical resolution (aside from the nominal one).

The Ekman layer depth does not seem to have the correct units

The discussion on how windage is computed should be introduced for consistency in Section 2.2 (before eq 5). How are the two r parameter values used in the paper (0.01.5, 0.005) obtained? The authors mention a quite extensive range from the literature; how did they select the two values and did they do some sensitivity tests?

How is the Smagorinsky diffusion coefficient computed? from the geostrophic velocity?

Thank you for these helpful comments. We agree that the original explanations of the datasets and numerical schemes in Sections 2.2 and 2.3 were incomplete. We have revised these sections to provide clearer descriptions of the SEALEVEL product, Ekman layer depth, windage parameterization, and Smagorinsky diffusion coefficient.

(1) SEALEVEL product

We have added more details on the SEALEVEL product in Section 2.2. The geostrophic current used in this study was derived from the Copernicus Marine SEALEVEL Level-4 altimeter product processed by the CNES/CLS DUACS multimission altimeter data processing system. This product is based on merged satellite altimeter observations and provides sea level anomaly, absolute dynamic topography, and derived geostrophic currents. We now explicitly state that the product combines observations from multiple satellite altimeter missions, including Sentinel-6A, Sentinel-3A/B, Jason-3, SARAL/AltiKa, CryoSat-2, OSTM/Jason-2, Jason-1, TOPEX/Poseidon, Envisat, GFO, ERS-1/2, and Haiyang-2A/B. The current Copernicus Marine SEALEVEL global Level-4 product is distributed on a nominal grid of 0.125° × 0.125° with daily temporal resolution, whereas the product version used at the time of our processing had a nominal grid of 0.25° × 0.25°. We also clarified that the nominal grid spacing should not be interpreted as the true physical resolution of the mapped altimetry field. Following the Copernicus Marine quality documentation, the effective resolution of the global Level-4 DUACS product is of mesoscale order, approximately 180 km and 33 days at mid-latitudes.

(2) Ekman layer depth

We thank the reviewer for pointing out the dimensional inconsistency. The Ekman layer depth formulation was adopted from Rypina et al. (2021), but the units of the empirical coefficient were not stated clearly in the original manuscript. The Ekman layer depth $d = \alpha \times |\vec{u}_{10}|/(sin\ (\phi))^{0.5}$, ρ is the water density, ϕ is the latitude, $\alpha = 3.2(s)$ is an empirical scaling coefficient, and z is water depth. We have revised the manuscript in Line 189.

(3) Windage coefficient

We have moved the windage discussion to Section 2.2 (Lines 148-176), before the total velocity formulation in Section 2.3, so that all forcing components are introduced consistently before they are combined in the particle tracking model. We also expanded the explanation of how the two windage coefficients were obtained.

For the undrogued DX drifter, the cylindrical body had a diameter of 0.09 m and a height of 0.30 m, with approximately 0.03–0.05 m protruding above the water surface. Thus, the projected area exposed to air was $A_a \approx 0.09 \times (0.03–0.05) = 0.0027–0.0045\ m^2$, whereas the submerged projected area was $A_w \approx 0.09 \times (0.25–0.27) = 0.0225–0.0243\ m^2$. Using standard air and seawater densities and $C_{d,a}/C_{d,w} \approx 1$, the estimated windage coefficient is $r_{DX} \approx 0.012–0.016$. Therefore, $r = 0.015$ was adopted for the DX drifters.

For the drogued DO drifters, the exposed area above the water surface was similar to that of the DX drifters, but the submerged drag area was much larger because of the drogue plate positioned near 2 m depth. To avoid double-counting the two perpendicular plates, we used one effective

projected drogue plate area: $A_{w,drogue} = 0.30 \times 0.30 = 0.09\ m^2$. The submerged cylindrical body contributed $A_{w,body} \approx 0.09 \times 0.26 = 0.0234\ m^2$. Thus, the total effective submerged projected area was $A_w \approx 0.0234 + 0.09 = 0.1134\ m^2$. This gives $r_{DO} \approx 0.0053–0.0069$ when $C_{d,a}/C_{d,w} \approx 1$ is used. Accordingly, $r = 0.005$ was adopted as a conservative geometry-based estimate for the DO drifters.

We also checked this estimate against published drag coefficients for drifter drag-area calculations. McCaffrey and Koeberle (2024) used $C_D = 0.74$ for cylindrical float elements and $C_D = 1.98$ for flat-plate drogue elements in their drifter drag-area analysis. Applying these values to the DO geometry gives $r_{DO} = \left[\rho_a(0.74A_a)/\rho_w\left(0.74A_{w,body} + 1.98A_{w,drogue}\right)\right]^{1/2}$, which yields $r_{DO} \approx 0.0035–0.0045$. This is slightly lower than, but close to, the adopted value of $r = 0.005$. Therefore, $r = 0.005$ does not underestimate the direct wind effect on the DO drifters; rather, it provides a physically reasonable and slightly conservative estimate.

We agree that the windage coefficient is associated with uncertainty. However, we did not tune r to minimize trajectory error, because doing so would mix two different objectives: estimating a drifter-specific windage coefficient and evaluating the relative contributions of geostrophic current, Ekman current, Stokes drift, and windage. Instead, we used *a priori* geometry-based values of r and kept them fixed across the forcing-combination experiments. In response to the reviewer's comment, we added a sensitivity test for the undrogued DX drifter, which is more directly exposed to wind forcing. The geometry-based windage coefficient used for DX in the manuscript was $r = 0.015$. To examine the sensitivity of the results to this parameter, we repeated the DX simulations using a smaller value, $r = 0.005$, representing an underestimated windage effect, and a larger value, $r = 0.030$, representing an overestimated windage effect. The sensitivity test showed that the optimal forcing combination changed when r was substantially modified. For $r = 0.005$, the lowest average MAE was obtained for C8, $u_g + u_e + u_s + u_w$, with $\overline{MAE} = 117.3$ km. For the geometry-based value, $r = 0.015$, the lowest average MAE was obtained for C7, $u_g + u_s + u_w$, with $\overline{MAE} = 42.9$ km. For $r = 0.030$, the lowest average MAE was obtained for C4, $u_g + u_w$, with $\overline{MAE} = 88.2$ km. Although different values of r produced different optimal forcing combinations, the geometry-based value $r = 0.015$ produced the smallest overall error among the tested cases. Specifically, the optimal MAE values for $r = 0.005$ and $r = 0.030$ were 117.3 km and 88.2 km, respectively, both of which were larger than the optimal MAE of 42.9 km obtained using $r = 0.015$. These results indicate that model performance is sensitive to the windage coefficient, but they also support the use of the geometry-based value $r = 0.015$ for the DX drifter. We therefore used the geometry-based coefficient as the primary estimate and used the additional simulations only to evaluate sensitivity, rather than tuning r freely to obtain the best trajectory fit. This clarification have been added to the revised manuscript in Lines 477-479.

Table R1. MAE values for PTM-DX sensitivity test using $r = 0.005$.

Day	C1	C2	C3	C4	C5	C6	C7	C8
5	130.2	128.2	123.1	129.8	106.3	117.1	90.0	29.2

Day	C1	C2	C3	C4	C5	C6	C7	C8
10	252.4	243.2	223.7	237.2	207.1	220.9	166.0	138.2
30	473.4	449.3	300.2	423.5	260.2	348.0	209.0	161.1
75	550.2	541.3	290.9	459.2	219.8	369.3	145.0	140.7
Avg.	351.6	340.5	234.5	249.9	198.4	211.1	122.0	117.3

Table R2. MAE values for PTM-DX sensitivity test using the geometry-based value $r = 0.015$.

Day	C1	C2	C3	C4	C5	C6	C7	C8
5	130.2	128.2	123.1	89.0	106.3	60.9	25.3	20.4
10	252.4	243.2	223.7	162.3	207.1	104.5	29.5	43.9
30	473.4	449.3	300.2	216.4	260.2	104.6	55.6	114.0
75	550.2	541.3	290.9	164.6	219.8	98.3	61.2	105.4
Avg.	351.6	340.5	234.5	158.1	198.4	92.1	42.9	70.9

Table R3. MAE values for PTM-DX sensitivity test using $r = 0.030$.

Day	C1	C2	C3	C4	C5	C6	C7	C8
5	130.2	128.2	123.1	**25.6**	106.3	31.8	48.4	58.6
10	252.4	243.2	223.7	**69.8**	207.1	87.2	117.7	109.7
30	473.4	449.3	300.2	**131.9**	260.2	165.9	207.7	198.8
75	550.2	541.3	290.9	**125.5**	219.8	173.7	207.7	198.8
Avg.	351.6	340.5	234.5	**88.2**	198.4	91.7	116.3	113.2

(4) Smagorinsky diffusion

We have clarified how the Smagorinsky diffusion coefficient was computed. The horizontal diffusivity was calculated from the same velocity field used in each PTM experiment, not only from the geostrophic current. Thus, for the geostrophic-only case, the Smagorinsky coefficient was computed from the geostrophic velocity field, whereas for combined forcing cases it was computed from the corresponding total velocity field (Lines 218-219).

4. The authors mention (line 169 pg 6) that in order to evaluate the PTM versus drifter motion they compute one numerical particle for each drifter initial location. They should clarify whether they actually use an ensemble of particles obtained varying the gaussian random number. Using only one particle, corresponding to a single random realization, would not make sense, and they should repeat the tests using an appropriate ensemble

Thank you for this important comment. We agree that using only one numerical particle for each drifter initial location may make the comparison sensitive to a single stochastic realization of the

random-walk diffusion term. We therefore repeated the PTM simulations using an ensemble of 10 numerical particles for each drifter initial location. The model–drifter comparison was then recalculated using the ensemble-mean MAE.

We show the original single-particle MAE table (Table R2) and the revised 10-particle ensemble-mean MAE table (Table R3). The absolute MAE values changed slightly because of the stochastic diffusion term, but the main optimal forcing combinations remained unchanged. For PTM-DX, C8 produced the lowest MAE at the early time of 5 days, whereas C7 produced the lowest MAE at later times and also had the lowest average MAE. Thus, except for the very early stage (~5 days), C7 remained the optimal forcing combination for DX. For PTM-DO, C8 consistently produced the lowest MAE in both the original single-particle case and the 10-particle ensemble case. We mentioned this in lines 508-514.

We also found a formatting error in the original manuscript table: for PTM-DX at 5 days, C7 had been incorrectly marked in bold as the best-performing case, although C8 actually had the lowest MAE at that time. This error has been corrected in the revised manuscript.

Table R2. Original MAE table using one numerical particle per drifter initial location.

	Day	C1	C2	C3	C4	C5	C6	C7	C8
PTM-DX	5	134.5	107.3	122.7	90	106.1	57	22	**19.3**
	10	251.4	242.6	221.1	166	209.6	92.6	**24.1**	35.8
	30	475.8	460.7	308.6	209	265.6	92	**54**	91
	75	562.5	606.1	347	145	243.9	90.8	**73.8**	83.2
PTM-DO	5	75.7	64.1	79.3	68.7	68.8	59.2	68.7	**55.3**
	10	146.5	135.6	140.2	123.1	129.4	113.8	120.1	**107**
	30	318	286.5	304.9	235.6	216.9	175.5	201.4	**110.7**
	75	537	487.9	487.9	377.1	459.6	322.6	410.3	**185.2**

Table R3. Revised MAE table using a 10-particle ensemble and ensemble-mean MAE.

	Day	C1	C2	C3	C4	C5	C6	C7	C8
PTM-DX	5	130.2	128.2	123.1	89	106.3	60.9	25.3	**20.4**
	10	252.4	243.2	223.7	162.3	207.1	104.5	**29.5**	43.9
	30	473.4	449.3	300.2	216.4	260.2	104.6	**55.6**	114
	75	550.2	541.3	290.9	164.6	219.8	98.3	**61.2**	105.4
PTM-DO	5	70.5	64.8	77.4	67	67.5	57.8	67.5	**53**
	10	142.9	133.5	143.1	125.7	129.4	114.3	120.1	**106**
	30	315.6	273.7	296.2	276	211	166.6	194.9	**117.7**
	75	528.1	488.7	477	472.9	359.2	285	330.9	**182.6**

5. How is the 'cluster' used in section 2.5 to compute relative dispersion defined? Is it given by the total set of drifters released, i.e. using six distinct deployment locations as a single point? Or is it an average of the six individual clusters? The behaviour at initial times seems strange to me

Thank you for pointing this out. We agree that the term "cluster" in Section 2.5 was not clearly defined and could therefore be misleading. Pairwise squared separation distances were first calculated among the available drifter trajectories, and only initially close drifter pairs with an initial separation distance of less than 200 m were retained. The relative dispersion and dispersion coefficient were then computed from this ensemble of initially close drifter pairs. This clarification has been added to Section 2.5 of the revised manuscript in Line 267.

6. The authors state that there is a Hyperbolic Point in the geostrophic velocity, causing the observed bifurcation. I think they should be more precise in their definition; they should look at the FSLE structure from the geostrophic velocity field to verify whether or not the bifurcation is indeed a HP.

Thank you for this important comment. In the revised manuscript, we clarified that the identification of the bifurcation region was not based solely on the instantaneous geostrophic velocity field. Instead, we examined the FTLE field derived from the geostrophic velocity and identified the spatial structure of the hyperbolic region using the red and blue FTLE ridges, which represent attracting and repelling manifolds, respectively (Shadden et al., 2005; Wiggins, 2005; Haller, 2015). Near the bifurcation region, the FTLE contours show a clear configuration of attracting and repelling ridges that is consistent with a hyperbolic Lagrangian structure. This ridge pattern supports our interpretation that the observed bifurcation was associated with a hyperbolic-point-like structure in the geostrophic flow field (Lines 296-301).

7. Also, the reason why the data driven combination outperform the one based on model velocity (Section 4) seems to be that the velocity bifurcation is not present in the model outputs. I find this strange, since the models should assimilate surface height and therefore induce a similar geostrophic velocity with respect to the altimetry products. Can the authors explain this point? And possibly compare the model velocities with the geostrophic one?

Thank you for this insightful comment. We agree that, because GLORYS and GOFS/HYCOM assimilate satellite altimetry, their large-scale sea-surface-height fields may contain information similar to that used to derive the altimetric geostrophic velocity. However, we found that the assimilated model products do not necessarily reproduce the same near-surface Lagrangian transport structure as the altimetry-derived geostrophic velocity. Therefore, even if the large-scale sea-surface-height signal is assimilated, the resulting large scale surface velocity gradients and finite-time transport barriers can differ from those obtained directly from the altimetry-derived geostrophic velocity.

We performed a direct comparison of the Lagrangian structures computed from the data-driven velocity combinations and from the model-derived velocity products using FTLE fields. The new figure shows that the data-driven velocity fields, especially G, GES, and GESW, contain a clear hyperbolic-type Lagrangian structure near the region where the observed drifter trajectories bifurcated. In contrast, the corresponding FTLE structures obtained from CMS and HYC are weaker, displaced, or less coherent in this region. Adding windage and Stokes drift to CMS and

HYC modifies the FTLE ridges, but it does not fully recover the same transport-separating structure seen in the data-driven velocity fields.

Thus, the better performance of the data-driven combinations is not simply because they contain an additional velocity component, but because they better reproduce the finite-time Lagrangian structure controlling the early separation of the drifter pathways. The comparison also indicates that assimilation of sea-surface height in GLORYS and GOFS/HYCOM does not guarantee that the model-derived surface velocity will reproduce the same geostrophic velocity gradients and hyperbolic-type transport structure as the altimetry-derived geostrophic product. We have clarified this point in the revised manuscript and added the FTLE comparison figure to support the interpretation (Lines 565-591)..

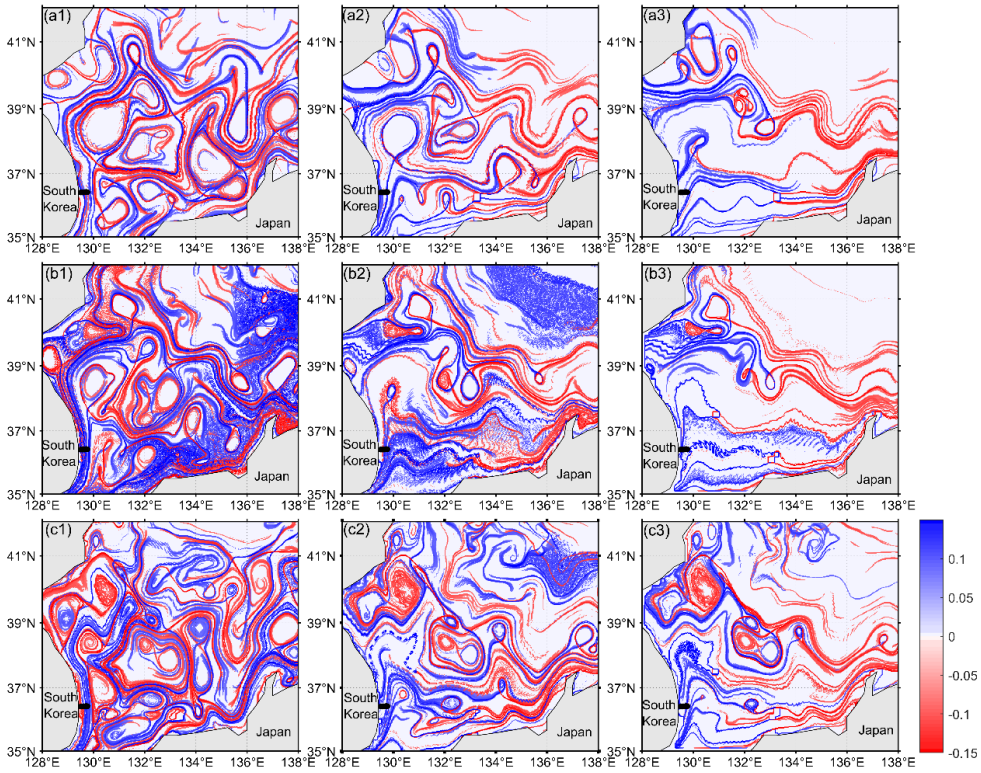

Figure 10. Finite-time Lyapunov exponent (FTLE) structures computed from one-week-averaged velocity fields. The panels show FTLE fields for (**a1**) u_g, (**a2**) $u_g + u_e + u_s$, (**a3**) $u_g + u_e + u_s + u_w$, (**b1**) CMS, (**b2**) CMS-w1, (**b3**) CMS-w1-st, (**c1**) HYC, (**c2**) HYC-w1, and (**c3**) HYC-w1-st. Here, u_g, u_e, u_s, and u_w denote geostrophic current, Ekman current, Stokes drift, and windage, respectively. CMS denotes the GLORYS reanalysis distributed by Copernicus Marine, and HYC denotes the GOFS analysis based on HYCOM.

8. Results from Ekman and windage (Section 3) are likely to strongly depend on parameterization and parameter values that are very difficult to evaluate. Did they do any sensitivity test? How robust are their conclusions?

Thank you for this important comment. We agree that the windage contribution can depend on the selected windage coefficient, r, and that this uncertainty should be discussed explicitly.

We clarify that the Ekman current in this study was not treated as an empirical tuning parameter. It was calculated directly from the wind-stress-based Ekman formulation using the prescribed wind field, latitude, and sampling depth. No additional adjustable coefficient was introduced for the Ekman current in the PTM simulations. Therefore, we did not perform a separate parameter sensitivity test for the Ekman component.

In contrast, windage was parameterized using the windage coefficient, r. In the main simulations, we used geometry-based estimates of $r = 0.015$ for the undrogued DX drifters and $r = 0.005$ for the drogued DO drifters. These values were derived from the exposed and submerged projected areas of each drifter type, rather than tuned to improve trajectory skill.

We also note that broadly tuning r is not straightforward in this study because DX and DO represent two physically different drifter types. The DX drifter is more surface-exposed and is therefore expected to have stronger direct windage, whereas the DO drifter has a larger submerged drogue area and is expected to have weaker direct windage. If r is varied too broadly for both drifter types, the parameter range of one drifter type can overlap with that of the other. Such tuning would blur the physical distinction between the DX and DO datasets and would mix two different objectives: calibrating a drifter-specific windage coefficient and evaluating the relative roles of geostrophic current, Ekman current, Stokes drift, and windage.

To evaluate the robustness of the DX results without treating r as a free tuning parameter, we conducted a limited windage sensitivity test for the DX case using three representative values: $r = 0.005$ as a lower-bound windage case, $r = 0.015$ as the geometry-based DX estimate, and $r = 0.030$ as an upper-bound windage case. The sensitivity test showed that the absolute trajectory errors varied with r, as expected. The use of $r = 0.015$, estimated from the DX drifter geometry, gave C7 ($u_G + u_S + u_W$) as the optimal forcing combination. When windage was underestimated using $r = 0.005$, the optimal combination shifted to C8 ($u_G + u_E + u_S + u_W$), suggesting that the weakened direct windage term was partly compensated by the inclusion of Ekman current. In contrast, when windage was overestimated using $r = 0.030$, the optimal combination shifted to C3 ($u_G + u_S$), indicating that excessive direct windage degraded the trajectory simulation and that the model favored a windage-free configuration. This indicates that the exact ranking of forcing combinations is sensitive to unrealistic underestimation or overestimation of r, but the geometry-based value $r = 0.015$ provides the most physically consistent representation of the DX drifter. More importantly, the sensitivity test supports the main conclusion that direct windage is an essential component for the surface-exposed DX drifters, but it should be constrained by drifter geometry rather than freely tuned to optimize trajectory skill.

We have added this to the revised manuscript in Lines 472-479.

9. I cannot see Tab 1-2 in the text

We apologize for this oversight. Tables 1 and 2 were inadvertently omitted from the original manuscript text. We have now added both tables to the revised manuscript and ensured that they are properly cited in the relevant sections.

More specific points

1. The definition of PTM should be better clarified when introduced in pg 2. There is a great variety of particle models; often they are based on Eulerian velocity from models outputs, and various types of stochastic terms are considered. In some cases stochastic terms are actually not used at all, if the velocity is assumed to be known with sufficient accuracy, for instance with high resolution models or HF Radars. I think the authors should clarify first of all that they do not include plastic behaviour (see point 1)), and that they use a simple random walk model (eq 4), and focus on Eulerian velocities based on various data sets, each capturing a specific transport processes (geostrophic, Ekman, windage, Stokes drift). Only as a second step they also test model results.

Thank you for this helpful comment. We agree that the definition and scope of the PTM used in this study should be clarified. In the revised manuscript, we have added a clearer explanation when PTM is first introduced. Specifically, we now state that PTMs can be based on Eulerian velocity fields from observations or numerical models, and that stochastic terms may or may not be included depending on the application and the accuracy of the velocity fields. We also clarified that our study does not include plastic-specific behaviors such as sinking, fragmentation, buoyancy changes, or beaching. Instead, the simulated particles are treated as passive floating drifters.

In addition, we revised the description of Eq. (4) to state that our model uses a simple random walk scheme to represent unresolved subgrid-scale diffusion. We also clarified that the main focus of the study is the use of data-driven Eulerian velocity components, including geostrophic current, Ekman current, windage, and Stokes drift. The model-derived velocity products are then tested as an additional comparison, rather than being the main focus of the study (Lines 699-700, 717-720).

2. Figures should be improved. In Fig.1 it would be useful to have an insert that locates the geographic area. Also, the names of the various lands should be indicated in all the figures, and consistency should be maintained between Fig.1, 2,5, 6 (in terms of area, schematic, data sources, coordinates, names etc..) Also, the arrows in Fig.1b,c are not well visible.

Thank you for these helpful comments. We agree that the figures should be improved for clarity and consistency. In the revised manuscript, we have updated Figures 1 and 2. We apologize that Figures 5 and 6 have not yet been fully revised, but we will update them.

3. Please check for typos. Some examples are:

line 75, (pg 3,) TO validate

line 101(pg 4) THE drifters (instead of these).

title of Section 3 (line 208, pg 8)

Thank you for your detailed comment. We have carefully reviewed the manuscript and corrected the typographical and grammatical errors.

References

Davis, R. E.: Drifter observations of coastal surface currents during CODE: The method and descriptive view, Journal of Geophysical Research: Oceans, 90(C3), 4741–4755, 1985. https://doi.org/10.1029/JC090iC03p04741

Haller, G. (2015). Lagrangian coherent structures. *Annual Review of Fluid Mechanics*, 47, 137–162.

Novelli, G., Guigand, C., Cousin, C., Ryan, E. H., Laxague, N. J. M., Dai, H., Haus, B. K., and Özgökmen, T. M.: A biodegradable surface drifter for ocean sampling on a massive scale, Journal of Atmospheric and Oceanic Technology, 34(11), 2509–2532, 2017. https://doi.org/10.1175/JTECH-D-17-0055.1

Poulain, P.-M. and Gerin, R.: Assessment of the water-following capabilities of CODE drifters based on direct relative flow measurements, Journal of Atmospheric and Oceanic Technology, 36, 621–633, 2019. https://doi.org/10.1175/JTECH-D-18-0097.1

Poulain, P.-M., Centurioni, L. R., and Özgökmen, T. M.: Comparing the currents measured by CARTHE, CODE and SVP drifters as a function of wind and wave conditions in the southwestern Mediterranean Sea, Sensors, 22, 353, 2022. https://doi.org/10.3390/s22010353

Shadden, S. C., Lekien, F., and Marsden, J. E. (2005). Definition and properties of Lagrangian coherent structures from finite-time Lyapunov exponents in two-dimensional aperiodic flows. *Physica D: Nonlinear Phenomena*, 212, 271–304.

Wiggins, S. (2005). The dynamical systems approach to Lagrangian transport in oceanic flows. *Annual Review of Fluid Mechanics*, 37, 295–328.